Available online at www.sciencedirect.com
ScienceDirect
International Journal of Heat and Mass Transfer 51 (2008) 1613–1627
International Journal of HEAT and MASS TRANSFER
www.elsevier.com/locate/ijhmt

Numerical analysis of natural convection heat transfer in a horizontal annulus partially filled with a fluid-saturated porous substrate

Khalil Khanafer [a], Abdalla Al-Amiri [b], Ioan Pop [c,*]

[a] *Biomedical Engineering Department, University of Michigan, Ann Arbor, MI 48109, USA*
[b] *Mechanical Engineering Department, United Arab Emirates University, United Arab Emirates*
[c] *Faculty of Mathematics, University of Cluj, R-3400 Cluj, Romania*

Received 10 April 2007; received in revised form 11 July 2007
Available online 10 October 2007

Abstract

The current study centers around a numerical investigation of natural convection heat transfer within a two-dimensional, horizontal annulus that is partially filled with a fluid-saturated porous medium. In addition, the porous sleeve is considered to be press fitted to the inner surface of the outer cylinder. Both cylinders are maintained at constant and uniform temperatures with the inner cylinder being subjected to a relatively higher temperature than the outer one. Moreover, the Forchheimer and Brinkman effects are taken into consideration when simulating the fluid motion inside the porous sleeve. Furthermore, the local thermal equilibrium condition is assumed to be applicable for the current investigation. The working fluid is air while copper is used to represent the solid phase. The porosity is considered to be uniform and constant with $\varepsilon = 0.9$. The main objective of this study is to examine the effect of the porous sleeve on the buoyancy induced flow motion under steady-state condition. Such an effect is studied using the following dimensionless parameters: $Pr = 0.05$–50, $Ra = 10^2$–10^6 and $Da = 10^{-4}$–10^{-6}. Also, the study highlights the effect of the dimensionless porous sleeve thickness (b) and thermal conductivity ratio (k_s/k_f) in the range between 1.1–1.9 and 1–150, respectively.

1. Introduction

Buoyancy-driven flow and heat transfer between horizontal concentric cylinders filled with a porous medium has been the subject of many investigations in recent years. The motivation for these studies was derived from their technological applications such as thermal insulation, thermal storage systems, nuclear reactors, underground electrical transmission lines (see, for example, Carrier-Mojtabi [1]). Many significant aspects of transport phenomena in porous media were discussed in recent monographs by Nield and Bejan [2], Ingham and Pop [3], Vafai [4,5], Vafai and Hadim [6], Ingham et al. [7], and Bejan et al. [8]. Caltagirone [9,10] conducted an extensive numerical analysis of steady-state natural convection in an annulus filled with a porous medium using both a perturbation method and a finite difference technique. It was reported that a fluctuating three-dimensional regime in the upper part of the porous layer was observed even though the lower part remained strictly two-dimensional. In a related work, Burns and Tien [11] analyzed natural convection in concentric spheres and horizontal cylinders filled with a porous medium. In addition, Rao et al. [12,13] solved the Boussinesq equations in two and three dimensions using the Galerkin finite element method. Three possible numerical solutions depending on the initial conditions were obtained for a radius ratio of 2 and Rayleigh numbers above 65. Moreover, Stewart and Burns [14] analyzed numerically the effect of a permeable inner boundary on the maximum temperature and the convective flows for a two-dimensional horizontal annulus containing a uniformly heat

* Corresponding author. Tel.: +40 264 594 315; fax: +40 264 591 906.
E-mail address: pop.ioan@yahoo.co.uk (I. Pop).

0017-9310/$ - see front matter © 2007 Elsevier Ltd. All rights reserved.
doi:10.1016/j.ijheatmasstransfer.2007.07.050

Nomenclature

b	dimensionless porous sleeve thickness, R_{porous}/R_i
c_p	specific heat at constant pressure, J m^{-1} K^{-1}
Da	Dacry number, K/R_i^2
$\mathbf{e}_r$, $\mathbf{e}_\phi$	unit vectors in the radial and angular directions, respectively
F	Forchheimer constant
g	gravitational acceleration, m s^{-2}
Gr	Grashof number, $g\beta\Delta TR_i^3/\nu^2$
$\mathbf{J}$	unit vector oriented along the pore velocity vector
k	thermal conductivity, W m^{-1} K^{-1}
K	permeability, m^2
L	length of the annulus, m
Nu	Nusselt number
$\overline{Nu}$	average Nusselt number, defined in Eq. (13)
p	pressure, N m^{-2}
P	dimensionless pressure
Pr	Prandtl number, ν/α
Q	total heat transfer, W
r	radial coordinate
R	dimensionless radial coordinate
R_i	radius of the inner cylinder
R_o	radius of the outer cylinder
R_{porous}	radius of the porous sleeve, m
Ra	Rayleigh number, $Gr\cdot Pr$
t	time, s
T	temperature, K
$\mathbf{v}$	dimensional pore velocity vector
V	dimensionless pore velocity vector

Greek symbols

α	thermal diffusivity, m^2 s^{-1}
β	thermal expansion coefficient, K^{-1}
ε	porosity
ϕ	angular coordinate
μ	fluid dynamic viscosity, kg m^{-1} s^{-1}
θ	dimensionless temperature, $(T-T_o)/(T_i-T_o)$
ρ	density, kg m^{-3}
σ	heat capacity ratio, $\lfloor\varepsilon(\rho c_p)_f+(1-\varepsilon)(\rho c_p)_s\rfloor/(\rho c_p)_f$
τ	dimensionless time, $t\sqrt{g\beta\Delta TR_i}/R_i$

Subscripts

cond	conduction
eff	effective quantity
f	fluid phase
i	inner cylinder
o	outer cylinder
s	solid phase

generating porous media. They illustrated that multi-cellular flows occurred at the highest Rayleigh numbers investigated. Furthermore, inverted symmetry in flow patterns and temperature distributions were observed when the heated isothermal wall condition changed from one cylinder wall to another.

Pop et al. [15] analytically investigated transient natural convection in a horizontal concentric annulus filled with a porous medium assuming Darcy's law. The inner and outer cylinders were maintained at uniform temperatures. Asymptotic solutions for the inner layer, the outer layer, and the core were obtained for small elapsed times. The authors found that the core, for relatively high Rayleigh numbers, was stratified and not isothermal, which signals the presence of an overwhelming conduction heat transfer regime. Meanwhile, Vasseur et al. [16] presented a numerical study of two-dimensional laminar natural convection between horizontal concentric cylinders filled with a porous layer with internal heat generation using Darcy–Oberbeck–Boussinesq equations. Meanwhile, Charrier-Mojtabi [1] conducted a numerical investigation of two- and three-dimensional free convection flows in a horizontal annulus filled with a fluid-saturated porous medium. The study considered an annulus that is heated at the surface of the inner cylinder using a Fourier–Galerkin approximation for the periodic azimuthal and axial directions whereas a collocation-Chebyshev approximation was used in the confined radial direction. In this study, the Darcy–Boussinesq formulation was employed. Bifurcation points between two-dimensional uni-cellular flows and either two-dimensional multi-cellular or three-dimensional flows were determined numerically. Bau [17,18], assuming the validity of the Darcy–Oberbeck–Boussinesq's equations in the considered range of employed parameters, obtained analytical results for thermal convection in a horizontal, eccentric

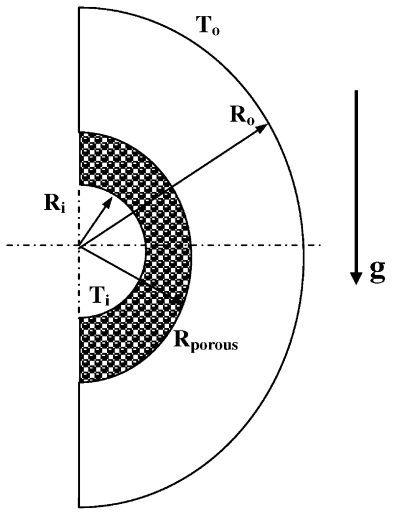

Fig. 1. Schematic of the physical model and coordinate system.

annulus containing a saturated porous medium using a regular perturbation expansion in terms of the Darcy–Rayleigh number. Further, the Nusselt number was expressed as a power series of Darcy–Rayleigh number for various eccentricity values. Mota and Saatdjian [19] studied numerically natural convection in a horizontal cylindrical annulus filled with a porous medium by solving the two-dimensional Boussinesq equations. A closed hysteresis loop was observed for radius ratios above 1.7 and for Rayleigh numbers above a critical value. The non-Darcian effects on natural convection in confined porous media between horizontal cylinders were studied by a number of authors including Kaviany [20]. The author illustrated that the effects of inertia, velocity-square and solid boundary terms reduced the total heat transfer rate with the boundary term being the most significant factor. A flow regime diagram showing the pseudo-conduction, Darcy, and non-Darcy regimes was given in that study.

Although a vast number of publications have analyzed natural convection in a horizontal annulus filled with a porous medium, less attention has been given to the problem of natural convection flow within a horizontal concentric annulus which is partially filled with a porous medium. Our survey of relevant literature indicated that Leong and Lai [21] obtained analytical solutions for natural convection in concentric cylinders with a porous sleeve using the

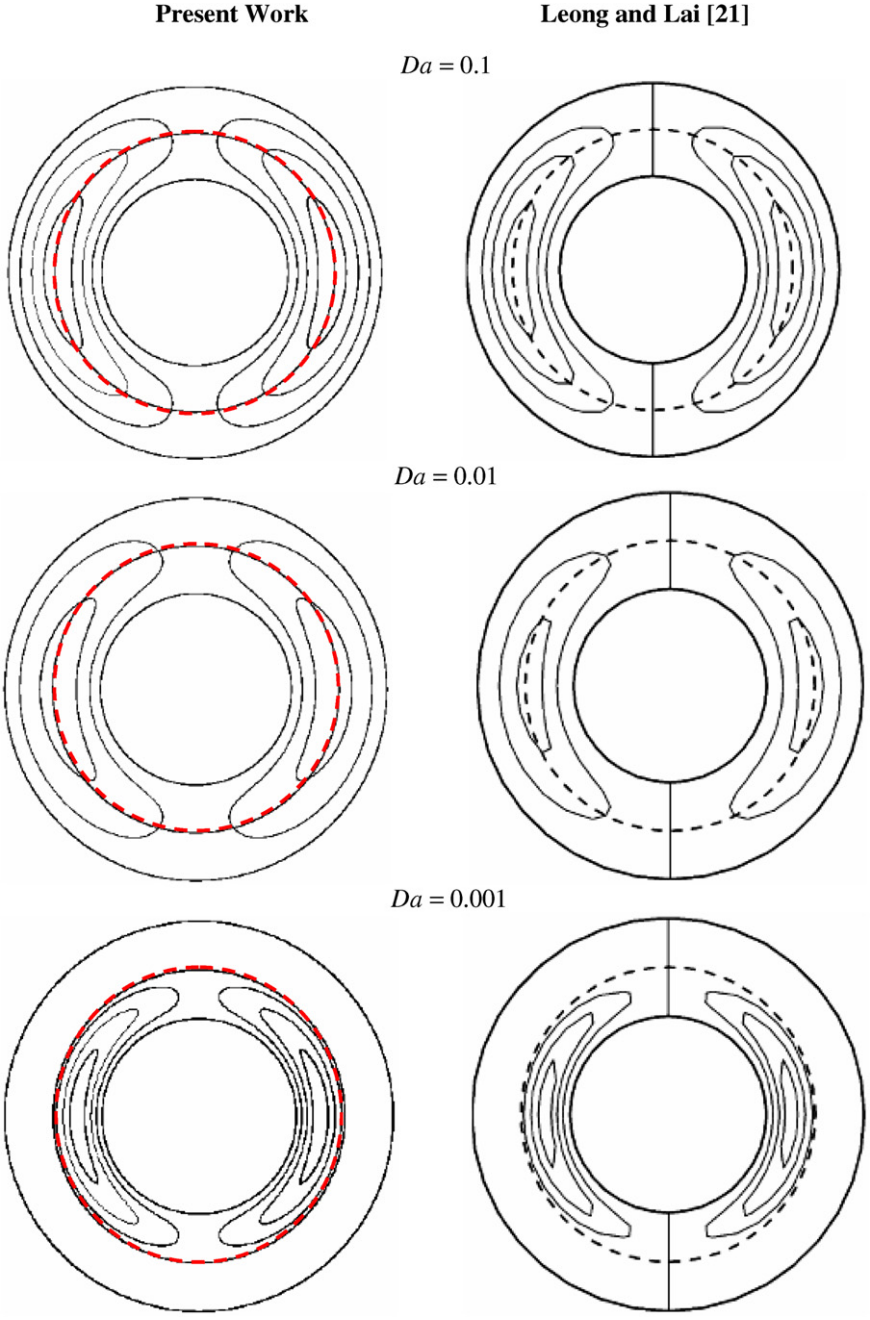

Fig. 2. Comparison of the streamlines between present work and that of Leong and Lai [21] ($Ra = 1$, $Pr = 2 \times 10^4$, $b = 1.5$, $k_s/k_f = 1$).

perturbation method and Fourier transform approach. The porous sleeve was press-fitted to the inner surface of the outer cylinder. Small temperature difference between the cylinders as well as small Rayleigh number were assumed in their investigation, which reflects the little convection activities attained within the annulus. The authors employed the extended Brinkman–Darcy's law to describe the flow motion inside the porous sleeve. Their results illustrated that for a sufficiently thin porous sleeve, the porous sleeve behaves as if it were impermeable. The study, however, did not recognize that the rigid matrix resistance cannot be prescribed by Darcy's law at high velocities owing to the appreciated increase in inertial effects.

The present study is focused on the analysis of the fluid flow and heat transfer within the annulus using a generalized form of the momentum equation that accounts for the porous medium viscous, Darcian and inertial effects. In addition, the undergoing investigation examines the effects of pertinent dimensionless parameters on the flow and heat transfer characteristics in the annulus. These

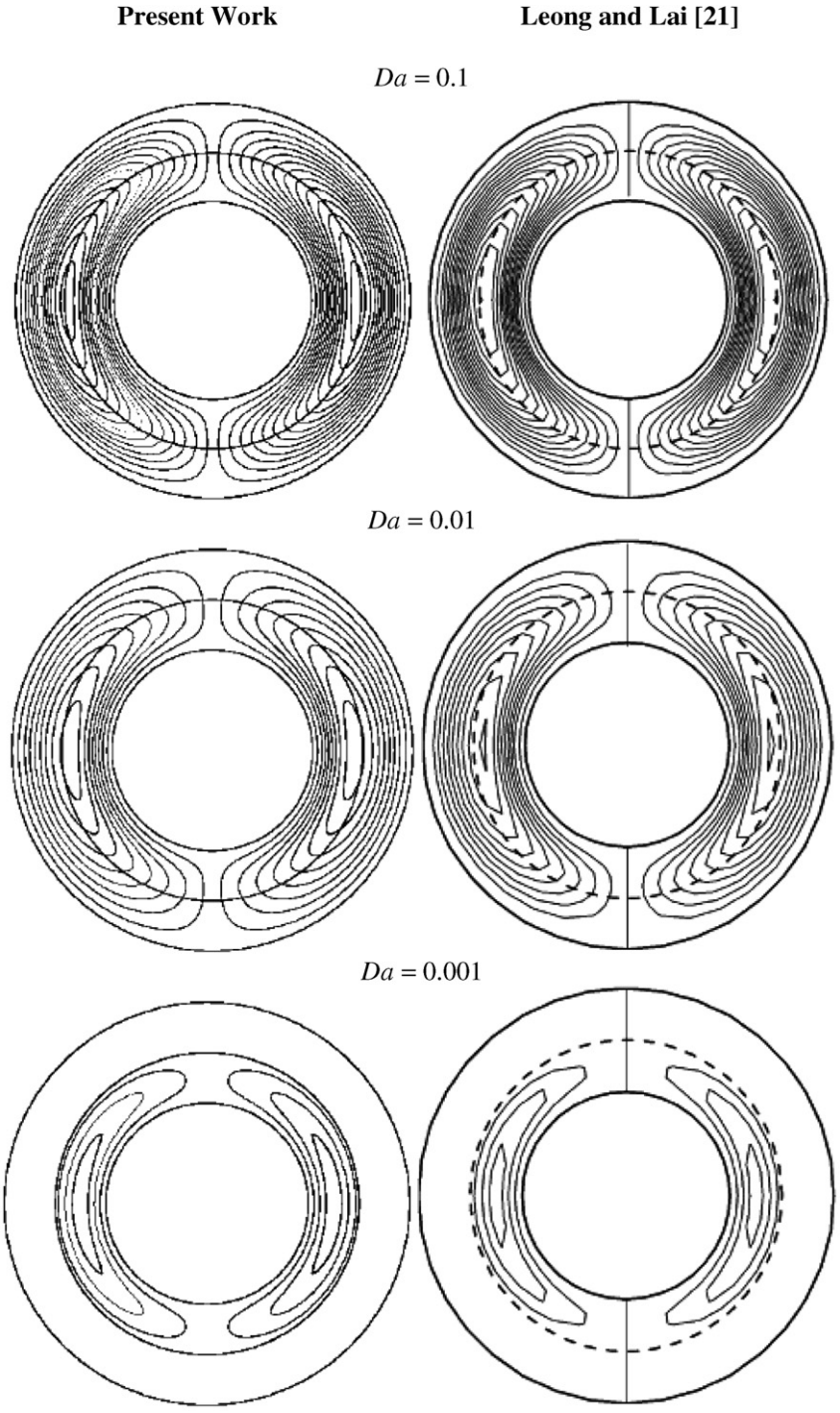

Fig. 3. Comparison of the streamlines between present work and that of Leong and Lai [21] ($Ra = 0.1$, $Pr = 2 \times 10^4$, $b = 1.5$, $k_s/k_f = 2$).

parameters are the Rayleigh number, Darcy number, porous sleeve thickness, Prandtl number and thermal conductivity ratio.

2. Mathematical formulation

The problem under investigation is a laminar two-dimensional natural heat transfer convection in a horizontal concentric annulus filled partially with a porous medium. The geometry of the problem under consideration and its coordinate system are shown in Fig. 1. In addition, the inner cylinder is of a radius R_i and the outer cylinder of a radius R_o are both kept at a uniform and constant temperatures T_i and T_o, respectively, while maintaining $T_i > T_o$. Moreover, the porous medium is viewed as a continuum with the solid and fluid phases in thermal equilibrium, isotropic, homogeneous, and saturated with an incompressible Newtonian fluid. Hence, the porous medium has a unique porosity ε and permeability K values. Furthermore, viscous heat dissipation in the fluid is assumed to be negligible in comparison to conduction and convection heat transfer effects. Also, it is assumed in the undergoing analyses that the thermophysical properties of the fluid are independent of temperature except for the density in the buoyancy term, which is treated according to the Boussinesq approximation. The governing equations in the porous sleeve are handled using the volume-average method.

By incorporating the above points, the system of the governing equations can be expressed in vectorial forms [22–25] as

Fluid layer:

$$\text{Continuity equation}: \nabla \cdot \boldsymbol{V} = 0 \tag{1}$$

$$\text{Momentum equation}: \frac{\partial \boldsymbol{V}}{\partial \tau} + \boldsymbol{V} \cdot \nabla \boldsymbol{V} = -\nabla P + \frac{1}{\sqrt{Gr}} \nabla^2 \boldsymbol{V} + \theta(\cos\phi \mathbf{e}_r - \sin\phi \mathbf{e}_\phi) \tag{2}$$

$$\text{Energy equation}: \frac{\partial \theta}{\partial \tau} + \boldsymbol{V} \cdot \nabla \theta = \frac{1}{Pr\sqrt{Gr}} \nabla^2 \theta \tag{3}$$

Porous sleeve:

$$\text{Continuity equation}: \nabla \cdot \langle \boldsymbol{V} \rangle = 0 \tag{4}$$

$$\text{Momentum equation}: \frac{1}{\varepsilon}\left[\frac{\partial \langle \boldsymbol{V} \rangle}{\partial t} + \langle (\boldsymbol{V} \cdot \nabla)\boldsymbol{V} \rangle\right] = -\nabla \langle P \rangle^f + \frac{1}{\varepsilon\sqrt{Gr}} \nabla^2 \langle \boldsymbol{V} \rangle - \frac{\langle \boldsymbol{V} \rangle}{Da\sqrt{Gr}} - \frac{F\varepsilon}{\sqrt{Da}} [\langle \boldsymbol{V} \rangle \cdot \langle \boldsymbol{V} \rangle]\mathbf{J} + \theta(\cos\phi \mathbf{e}_r - \sin\phi \mathbf{e}_\phi) \tag{5}$$

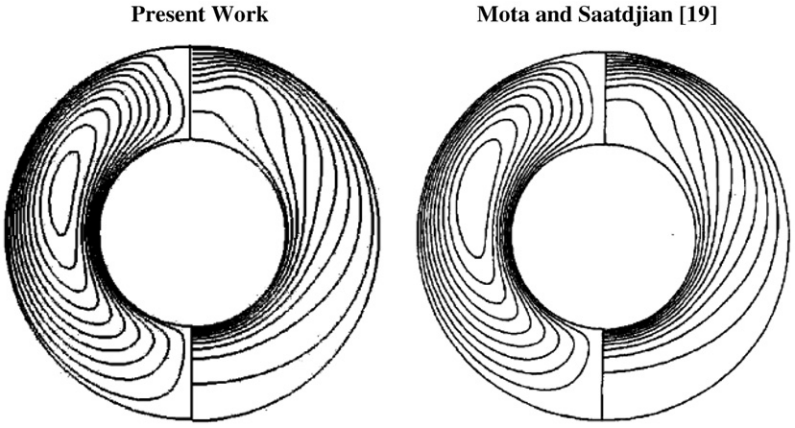

Fig. 4. Comparison of the streamlines and isotherms between the present work and that of Mota and Saatdjian [19] using $Ra = 100$ and $R_o/R_i = 2$.

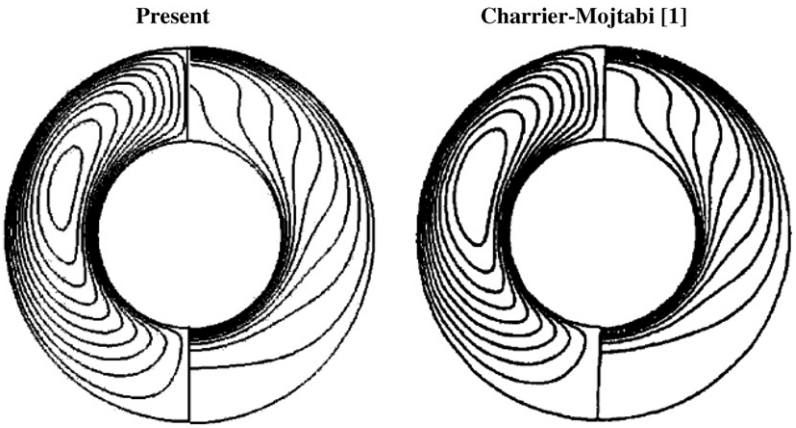

Fig. 5. Comparison of the streamlines and isotherms between the present work and that of Charrier-Mojtabi [1] using $Ra = 200$ and $R_o/R_i = 2$.

$$\text{Energy equation}: \sigma\frac{\partial\theta}{\partial\tau}+\boldsymbol{V}\cdot\nabla\theta=\frac{k_{\text{eff}}}{k_{\text{f}}}\frac{1}{Pr\sqrt{Gr}}\nabla^2\theta \tag{6}$$

where

$$k_{\text{eff}}=\varepsilon k_{\text{f}}+(1-\varepsilon)k_{\text{s}} \text{ and } \sigma = [\varepsilon(\rho c_p)_{\text{f}}+(1-\varepsilon)(\rho c_p)_{\text{s}}]/(\rho c_p)_{\text{f}} \tag{7}$$

The above equations were normalized using the following dimensionless parameters:

$$\boldsymbol{V}=\frac{\mathbf{v}}{\sqrt{g\beta\Delta TR_{\text{i}}}},\quad P=\frac{P}{\rho(g\beta\Delta TR_{\text{i}})},\quad \tau=\frac{t\sqrt{g\beta\Delta TR_{\text{i}}}}{R_{\text{i}}},$$
$$\theta=\frac{T-T_{\text{o}}}{T_{\text{i}}-T_{\text{o}}} \tag{8}$$
$$\boldsymbol{R}_{\text{i}}=\frac{R_{\text{i}}}{R_{\text{i}}}=1,\quad \boldsymbol{R}_{\text{o}}=\frac{R_{\text{o}}}{R_{\text{i}}},\quad b=\frac{R_{\text{porous}}}{R_{\text{i}}}$$

where β is the thermal expansion coefficient, ρ is the fluid density, g is the gravitational acceleration, $\mathbf{J}=V_{\text{p}}/|V_{\text{p}}|$ is a unit vector oriented along the pore velocity vector, P is the dimensionless pressure, $\boldsymbol{V}$ is the dimensionless velocity vector, $\mathbf{e}_{\text{r}}$ and $\mathbf{e}_{\phi}$ are the unit vectors in the radial and angular dimensions, respectively, $Da=K/R_{\text{i}}^2$ is the Darcy number and R_{porous} is the radius of the porous sleeve. In addition, the relevant Grashof number and Prandtl number are given by $Gr=g\beta\Delta TR_{\text{i}}^3/v^2$ and $Pr=v/\alpha$, respectively.

The boundary conditions for the problem under consideration are expressed as

$$\begin{aligned}&\boldsymbol{R}_{\text{i}}=1:\boldsymbol{V}=0,\quad \theta=1\\&\boldsymbol{R}_{\text{o}}=R_{\text{o}}/R_{\text{i}}:\boldsymbol{V}=\theta=0\end{aligned} \tag{9}$$

At the interface ($b=R_{\text{porous}}/R_{\text{i}}$):

$$\left(\frac{\partial\theta}{\partial R}\right)_{\text{f}}=\frac{k_{\text{eff}}}{k_{\text{f}}}\left(\frac{\partial\theta}{\partial R}\right)_{\text{p}} \text{ and } \left(\frac{\partial\boldsymbol{V}}{\partial R}\right)_{\text{f}}=\frac{\mu_{\text{eff}}}{\mu_{\text{f}}}\left(\frac{\partial\boldsymbol{V}}{\partial R}\right)_{\text{p}} \tag{10}$$
$$\theta_{\text{p}}=\theta_{\text{f}} \text{ and } \boldsymbol{V}_{\text{p}}=\boldsymbol{V}_{\text{f}}$$

where $\mu_{\text{eff}}=\mu_{\text{f}}/\varepsilon$.

The local Nusselt number distributions along the inner and outer cylinders are calculated as the actual heat transfer divided by the heat transfer for pure conduction in the absence of fluid motion as follows:

$$Nu_{\text{i}}(\phi)=\frac{Q_{\text{i}}}{Q_{\text{cond}}}=\frac{(2\pi RLk_{\text{eff}})\left(\frac{\partial T}{\partial r}\right)_{R_{\text{i}}}}{1/\left(2\pi Lk_f\ln\frac{R_{\text{o}}}{R_{\text{i}}}\right)}=-\frac{k_{\text{eff}}}{k_{\text{f}}}\left(\ln\frac{R_{\text{o}}}{R_{\text{i}}}\right)\left(R_{\text{i}}\frac{\partial T}{\partial r}\right)_{R_{\text{i}}} \tag{11}$$

$$Nu_{\text{o}}(\phi)=\frac{Q_{\text{o}}}{Q_{\text{cond}}}=\frac{(2\pi RLk_{\text{eff}})\left(\frac{\partial T}{\partial r}\right)_{R_{\text{o}}}}{1/\left(2\pi Lk_f\ln\frac{R_{\text{o}}}{R_{\text{i}}}\right)}=-\frac{k_{\text{eff}}}{k_{\text{f}}}\left(\ln\frac{R_{\text{o}}}{R_{\text{i}}}\right)\left(R_{\text{o}}\frac{\partial T}{\partial r}\right)_{R_{\text{o}}} \tag{12}$$

Meanwhile, the average Nusselt numbers estimated at the inner and outer cylinders are given by

$$\overline{Nu_{\text{i}}}=\frac{1}{2\pi}\int_0^{2\pi}Nu_{\text{i}}(\phi)\mathrm{d}\phi \quad \text{and}$$
$$\overline{Nu_{\text{o}}}=\frac{1}{2\pi}\int_0^{2\pi}Nu_{\text{o}}(\phi)\mathrm{d}\phi \tag{13}$$

Under steady-state conditions, both expressions in Eq. (13) should converge to the same result.

3. Numerical scheme

A finite element formulation based on the Galerkin method was utilized to solve the governing equations. The application of this technique is well documented by Taylor and Hood [26] and Gresho et al. [27]. In the current

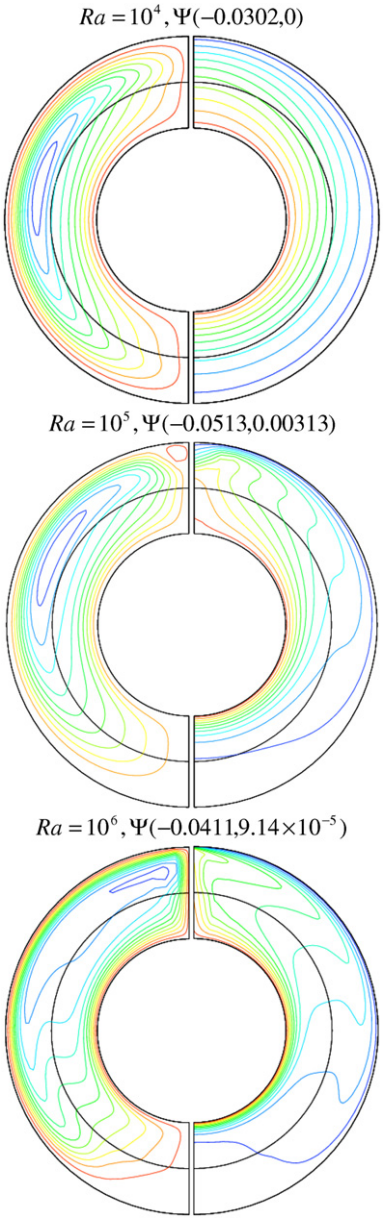

Fig. 6. Effect of varying Rayleigh number on the streamlines and isotherms using $b=1.5$, $k_{\text{s}}/k_{\text{f}}=1$ and $Da=10^{-3}$.

investigation, the continuum domain was divided into a set of non-overlapping regions called elements. Nine node quadrilateral elements with bi-quadratic interpolation functions were utilized to discretize the physical domain. Moreover, interpolation functions in terms of local normalized element coordinates were implemented to approximate the dependent variables within each element. Subsequently, substitution of the approximations into the system of the governing equations and boundary conditions yielded a residual for each of the conservation equations. These residuals were then reduced to zero in a weighted sense over each element volume using Galerkin method.

The highly coupled and non-linear algebraic equations resulting from the discretization of the governing equations were solved using an iterative solution scheme called the segregated-solution algorithm. The advantage of using this method lies in that the global system matrix is decomposed into smaller submatrices and then solved in a sequential manner. This technique results in considerably fewer storage requirements. A pressure projection algorithm was utilized to obtain a solution for the velocity field at every iteration step. Furthermore, the pressure projection version of the segregated algorithm was used to solve the non-linear system. In addition, the conjugate residual scheme was used to solve the symmetric pressure-type equation systems, while the conjugate gradient squared method was used for the non-symmetric advection-diffusion-type equations. The steady-state solution was assumed to be converged when the variation of the average Nusselt number between two consecutive time steps is less than 0.1%. The transient solution is advanced with a time step of 10^{-3} until steady-state solution is obtained.

4. Grid refinement

Many numerical experiments of various mesh sizes were performed to achieve grid-independent results and to determine the best compromise between accuracy and minimizing computer execution time. As such, a variable grid-size system was employed in the present work to capture the rapid changes in the dependent variables especially near the boundaries and the fluid-porous interface where the major gradients occur inside the boundary layer. To test and assess grid independence of the solution scheme, numerical experiments were performed for high Rayleigh number $Ra = 10^6$ using 40×40, 60×60 and 80×80 grid nodes, respectively. Based on the results, a grid system of 80×80 (non-uniform spacing) was adopted for all the cases completed in the present study. Further increase of the mesh size did not significantly change the final steady-state results for $Ra = 10^6$.

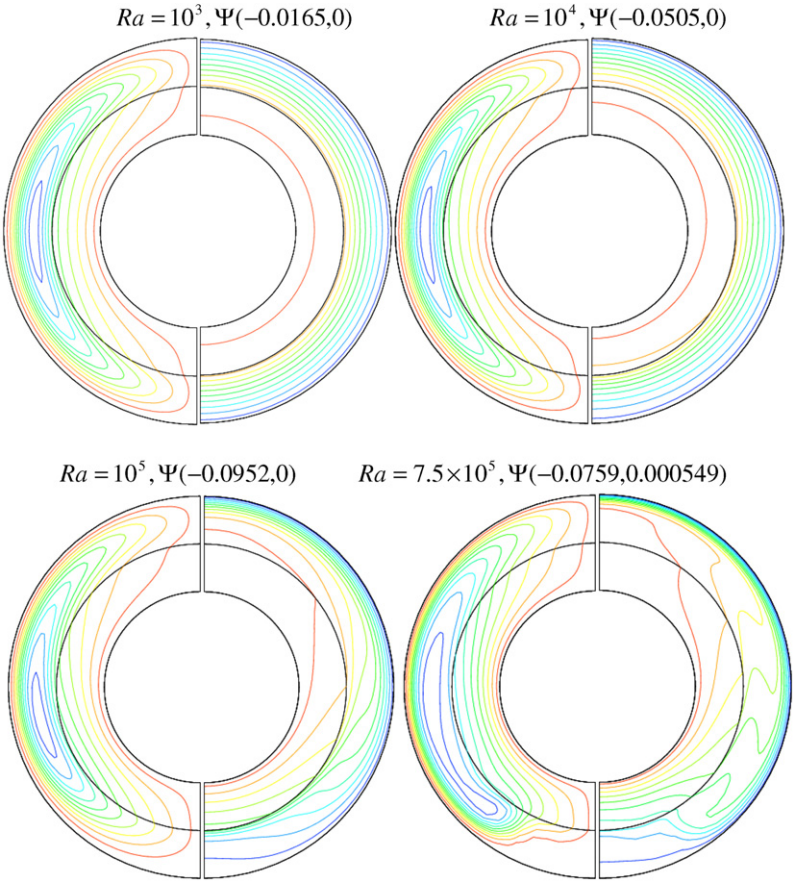

Fig. 7. Effect of varying Rayleigh number on the streamlines and isotherms using $b = 1.5$, $k_s/k_f = 100$ and $Da = 10^{-3}$.

5. Validation

The present numerical code was first validated against the analytical results of Leong and Lai [21] for natural convection in concentric cylinders with a porous sleeve. Figs. 2 and 3 illustrate a comparison of the streamlines and isotherms between the present code and the results of Leong and Lai [21] for various Rayleigh number, Darcy number, and thermal conductivity ratio. Both results were found in excellent agreement as depicted in Figs. 2 and 3. Moreover, the present numerical approach was validated against the numerical studies of Mota and Saatdjian [19] and Charrier-Mojtabi [1] in a porous horizontal cylindrical annulus for a radius ratio of 2 and Rayleigh numbers of 100 and 200 as shown in Figs. 4 and 5, respectively. These comparisons showed excellent agreements between the present results and other works available in the literature.

6. Results and discussion

The analyses in the undergoing numerical investigation are performed in the following domain of the associated dimensionless group: $Pr = 0.05$–50, $Ra = 10^3$–10^6, $Da = 10^{-4}$–10^{-6}, dimensionless porous sleeve thickness $b = 1.1$–1.9 and thermal conductivity ratio $k_s/k_f = 1$–150. The default case study in this investigation carried the following values: $\varepsilon = 0.9$, $b = 1.5$, $Da = 10^{-3}$, $k_s/k_f = 100$, $Pr = 1$ and $Ra = 10^4$. The results are presented in terms of the contour lines for the streamline and dimensionless temperature in one half of the annulus due to symmetry. In addition, average Nusselt number predictions are also documented for some cases.

6.1. Effect of Rayleigh number

Figs. 6 and 7 demonstrate the effect of varying the Rayleigh number on the streamline contours and isotherms for different conductivity ratios. The Rayleigh number reflects the strength of the imposed the temperature gradient between both cylinders in the annulus configuration. For a low Rayleigh number and a conductivity ratio of $k_s/k_f = 1$, Fig. 6 illustrates that the isotherms in both regions resemble eccentric circles which indicates pseudo-conductive regimes for fluid and porous sleeves since the overall heat transfer is essentially by conduction and the fluid motion driven by the buoyancy force is very slow. On the other hand, as Rayleigh number increases, the center of the circulation is driven upward and the isotherm contours are distorted resulting in an enhancement in the overall heat transfer. This is attributed to the fact that the thickness of the thermal boundary layer decreases along the

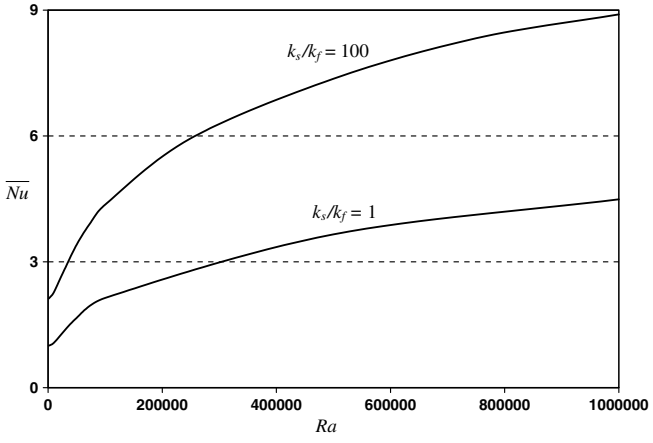

Fig. 8. Effect of varying Rayleigh number on the average Nusselt number for different conductivity ratio using $b = 1.5$ and $Da = 10^{-3}$.

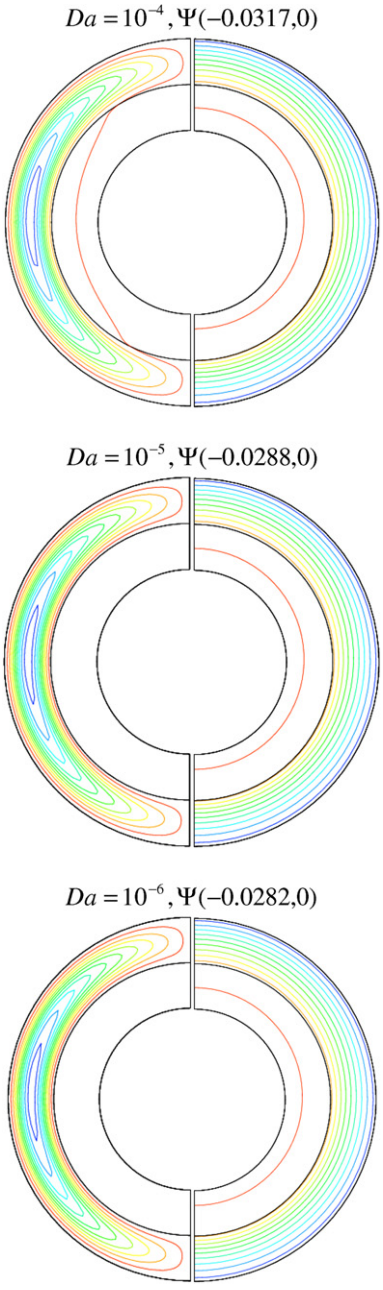

Fig. 9. Effect of varying Darcy number on the streamlines and isotherms using $b = 1.5$, $k_s/k_f = 100$ and $Ra = 10^4$.

inner cylinder with an increase in Rayleigh number. For the intermediate Rayleigh number used in this investigation, i.e., $Ra = 10^5$, flow activities enhances which leads to the formation of a vortex at the top portion of the annulus and a stagnant region at the lower portion of the annulus. The vortex, however, is not found to carry sufficient strength at $Ra = 10^5$ to become part of the main cell. As the Rayleigh number is increased further to $Ra = 10^6$, thinner boundary layers are shown to be presented along the inner and outer walls of the annulus owing to the domination of the buoyancy forces as compared to viscous forces. This leads to the formation of a turbulent boundary layer on the outer surface of the annulus as depicted in Fig. 6. This observation was reported in an earlier investigation by Lis [28]. The augmentation in the overall heat transfer activities is vivid from the additional contribution of the convection heat transfer as indicated by the distribution of the isotherms.

Fig. 7 illustrates the effect of Rayleigh number on the streamlines and isotherm contours for a higher thermal conductivity ratio of $k_s/k_f = 100$. The porous sleeve becomes more conductive than the fluid layer due to the magnitude difference in the thermal transport coefficient. For this particular reason, the porous sleeve is almost uniform in temperature at low Rayleigh numbers. For higher Rayleigh numbers, however, thinner boundary layer is

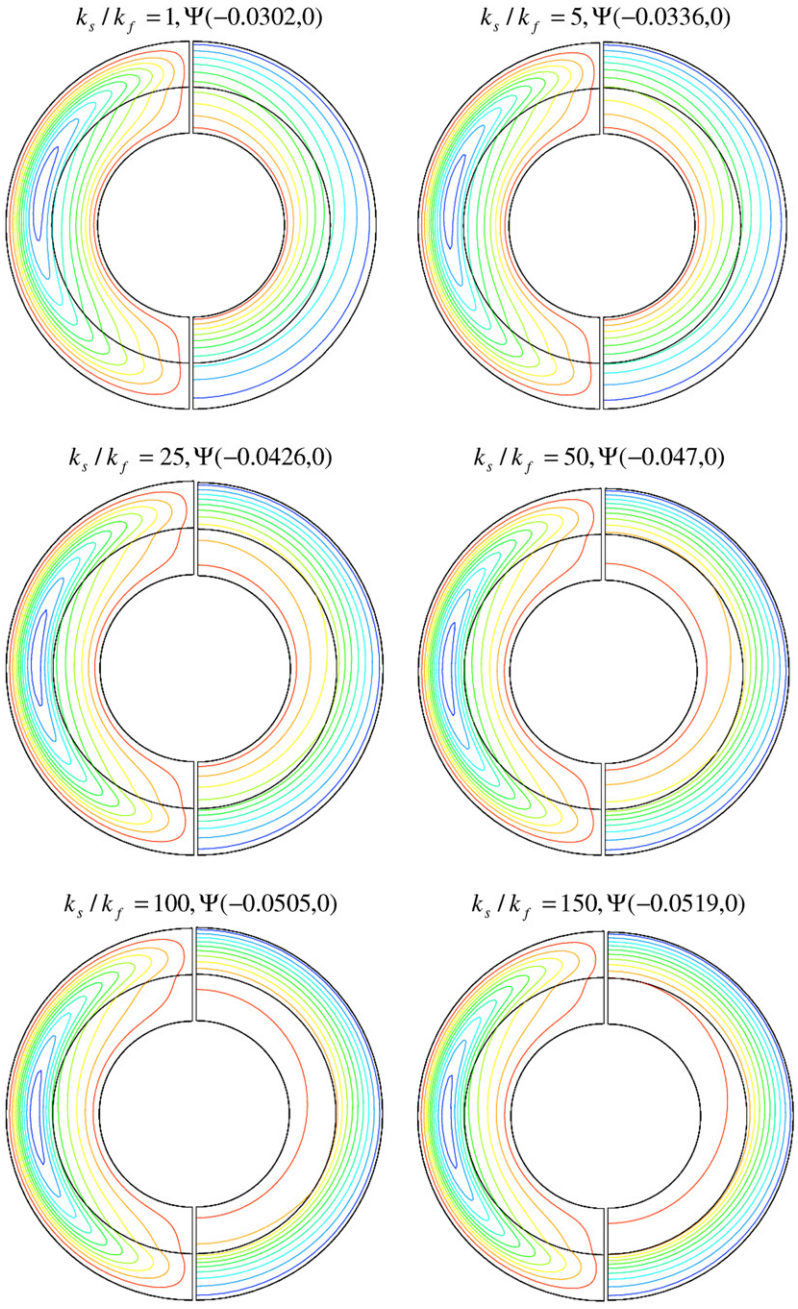

Fig. 10. Effect of varying the conductivity ratio on the streamlines and isotherms using $b = 1.5$, $Da = 10^{-3}$ and $Ra = 10^4$.

exhibited along the outer surface of the fluid layer indicating a large temperature gradient and consequently stronger convective flow activities in the fluid layer as depicted in Fig. 7. In the porous sleeve, the temperature fields depend mostly on the thermal conductivity for low Rayleigh number ($Ra \leqslant 10^4$) since heat conduction mechanism is dominant. However, for higher Rayleigh numbers ($Ra > 10^4$), the temperature fields in the porous sleeve depend on both the Rayleigh number and the conductivity ratio as shown in Fig. 7. This is confirmed in Fig. 8 which indicates the effect of varying Rayleigh number and conductivity ratio on the average Nusselt number. For a fixed Rayleigh number, the average Nusselt number is found to increase significantly with an increase in the conductivity ratio.

6.2. Effect of Darcy number

The effect of the Darcy number on the streamlines and isotherms is depicted in Fig. 9. For small values of the Darcy numbers, the fluid experiences a pronounced large resistance as it flows through the porous matrix causing the flow to cease in the porous sleeve as depicted in Fig. 9. It can be seen from this figure that as the Darcy number decreases, the porous sleeve is considered less permeable to fluid penetration and consequently, the convective activities are suppressed in the porous sleeve. This subsequently results in hindering flow activities in the fluid layer as well, which is reflected by the formation of the famous 'kidney-shaped' streamline cells. It is clearly noticed in Fig. 9 that the streamline contours are completely confined in the fluid layer for large conductivity ratio and small Darcy numbers. Meanwhile, the isotherm patterns indicate a pure conduction regime for the considered range of Darcy numbers as noted by the presence of thermal stratification in the radial direction of the fluid layer. Furthermore, the temperature is almost constant in the porous sleeve due to the high imposed thermal conductivity ratio, i.e., $k_s/k_f = 100$.

6.3. Effect of thermal conductivity ratio (k_s/k_f)

Fig. 10 illustrates the effect of varying the conductivity ratio on the streamlines and isotherms. It is apparent that as the conductivity ratio increases, the porous sleeve becomes more conductive than the fluid layer. As a result, the level of the circulation activity in the fluid layer increases due to a large fluid temperature gradient as indicated by the absolute values of the stream function. On the contrary, the strength of the convective flow in the porous sleeve decreases with an increase in the conductivity ratio leaving the porous sleeve almost isothermal as demonstrated in Fig. 10. It is worth noting that as the conductivity ratio increases, the spacing between the isotherms in the fluid layer decreases. Moreover, Fig. 11 illustrates the impact of the increase in the conductivity ratio on the average predicted Nusselt number. The overall heat transfer rate is enhanced with an increase in the thermal conductivity ratio due to large temperature gradients offered in the fluid layer. As such, the average Nusselt number increases rapidly for $k_s/k_f < 25$ as depicted from large slope of the average predicted Nusselt number. Thereafter, for $k_s/k_f > 25$, the average Nusselt number increases at a lower rate as indicated by the slope of the average Nusselt number.

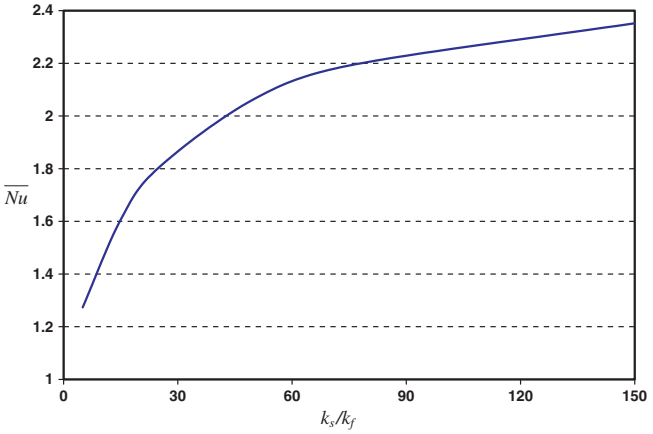

Fig. 11. Effect of varying thermal conductivity ratio on the average Nusselt number using $b = 1.5$, $Da = 10^{-3}$ and $Ra = 10^4$.

6.4. Effect of the porous sleeve thickness (b)

The combined effects of porous sleeve thickness and thermal conductivity ratio on the streamlines and isotherms can be examined from Figs. 12 and 13, respectively. For $k_s/k_f = 1$, Fig. 12 illustrates depreciation in the convection currents as the porous thickness increases. This is attributed to the increase in the offered flow resistance in the entire annulus which accordingly results in higher energy being lost through the flow resistance that subsequently leads to a weak convective flow in the annulus. Hence, the absolute values of the streamlines record a subsequent decrease with the increase in the porous sleeve thickness. In a nutshell, for a thermal conductivity ratio of unity, a thinner porous sleeve enhances convective activities within the fluid layer and, thus, permits better heat transfer since the porous sleeve is nearly impermeable and convection is primarily confined in the fluid layer. For a thicker porous sleeve of $b = 1.75$, the isotherms are eccentric and become almost concentric for a porous sleeve thickness of $b = 1.9$ indicating that the dominant heat transfer mechanism is conduction. This is associated with a fact that the presence of a porous medium within the annulus results in a force opposite to the flow direction which tends to hinder the flow motion. This consequently causes suppression in the thermal currents of the flow. This observation is manifested from the isotherm patterns as displayed in Fig. 12.

When considering a large conductivity ratio, i.e., $k_s/k_f = 100$, the fluid layer is less conductive than the porous sleeve and consequently the fluid layer will be subjected to

a large temperature gradient as shown in Fig. 13 while the temperature distribution is nearly uniform in the porous sleeve as depicted from the formation of a family of concentric isotherm circles. This is likely attributed to the fact that for a small Rayleigh number of $Ra = 10^4$ and a Darcy number of $Da = 10^{-3}$, the flow resistance becomes more significant and, therefore, it becomes more difficult for the convective flow to penetrate the porous sleeve, which leads to weaker convective cells.

6.5. Effect of Prandtl number

Next, the effect of Prandtl number (Pr) on the streamlines and isotherms is presented in Fig. 14 for a thermal conductivity ratio of $k_s/k_f = 100$ and a relatively small Darcy number of $Da = 10^{-3}$. This figure shows that Prandtl number has an impact on the intensity of the circulation within the annulus. At $Pr = 0.5$, the magnitude of the thermal diffusion (α) outweighs its momentum (ν) counter-

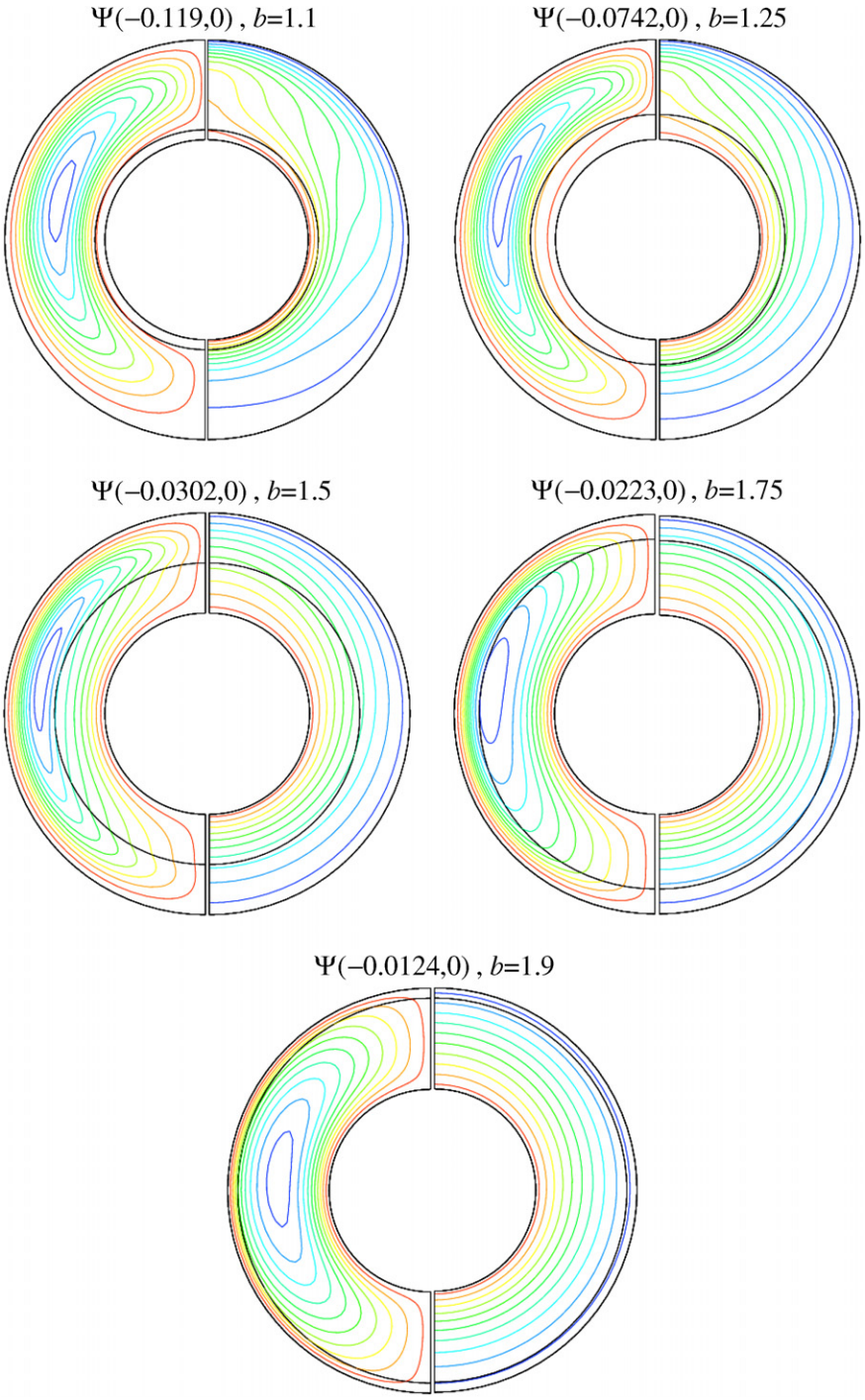

Fig. 12. Effect of varying the porous thickness on the streamlines and isotherms using $k_s/k_f = 1$, $Da = 10^{-3}$ and $Ra = 10^4$.

part causing notable flow activities, which is attributed to natural convection thermal currents. As Prandtl number increases, however, the momentum diffusion surpasses the thermal diffusion, which consequently dampens the convective flow within the annulus.

Overall, the Prandtl number does not seem to significantly impact the streamline and the isotherm distributions, at least, when employing small magnitudes of Rayleigh and Darcy numbers. The effect of Prandtl number can be further highlighted by plotting its impact on the average Nusselt number predications as demonstrated in Fig. 15. The average Nusselt number predications confirm our argument that $\overline{Nu}$ is less sensitive to variation in Pr values as compared to other dimensionless groups considered in this investigation. Moreover, the results show that $\overline{Nu}$ reaches an asymptotic value when $Pr > 1$. It is interesting to note that $\overline{Nu}$ predications at $k_s/k_f = 1$ can be doubled by increasing k_s/k_f by 100 folds.

6.6. Important observations on the average Nusselt number results

The undergoing investigation is wrapped by exploring the combined effects of porous sleeve thickness and thermal conductivity ratio on the average Nusselt number for various Rayleigh numbers. Fig. 16 shows that the average Nusselt number decreases with an increase in the porous sleeve thickness for a thermal conductivity ratio of unity

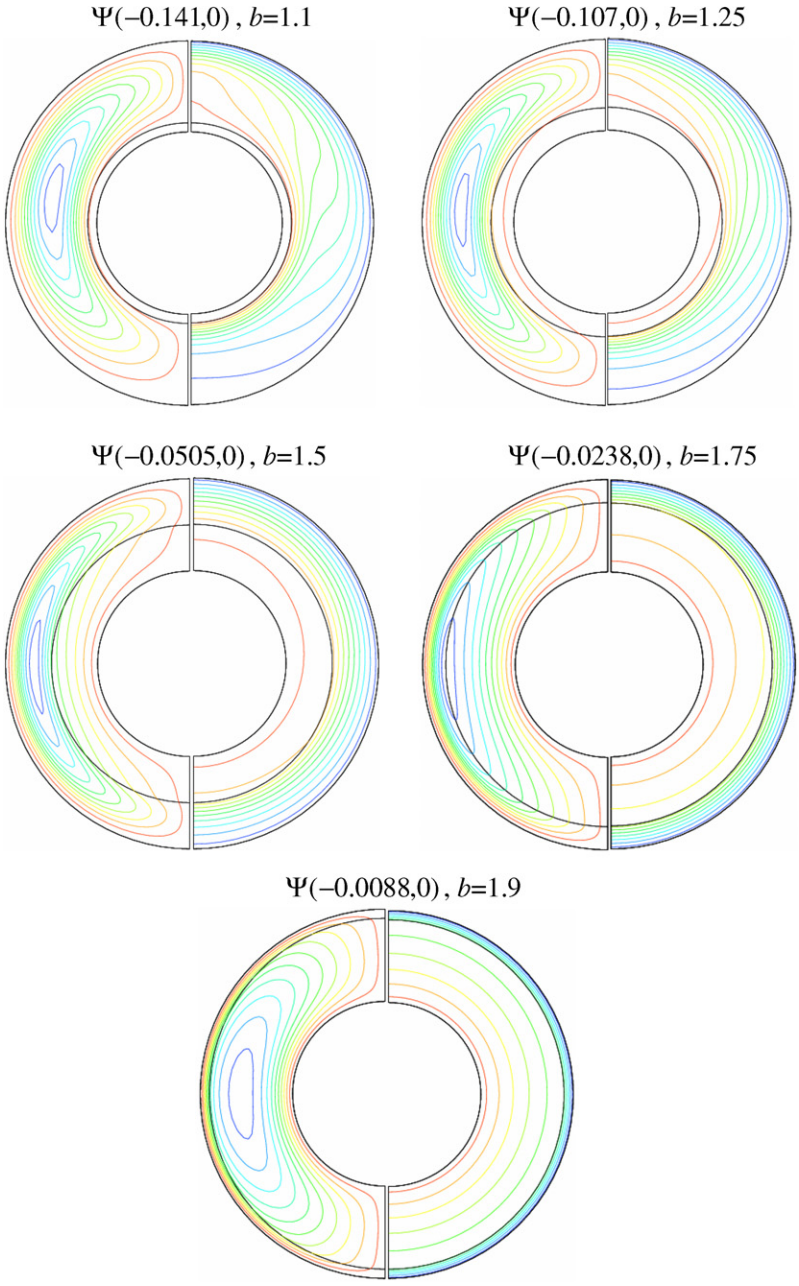

Fig. 13. Effect of varying the porous thickness on the streamlines and isotherms using $k_s/k_f = 100$, $Da = 10^{-3}$ and $Ra = 10^4$.

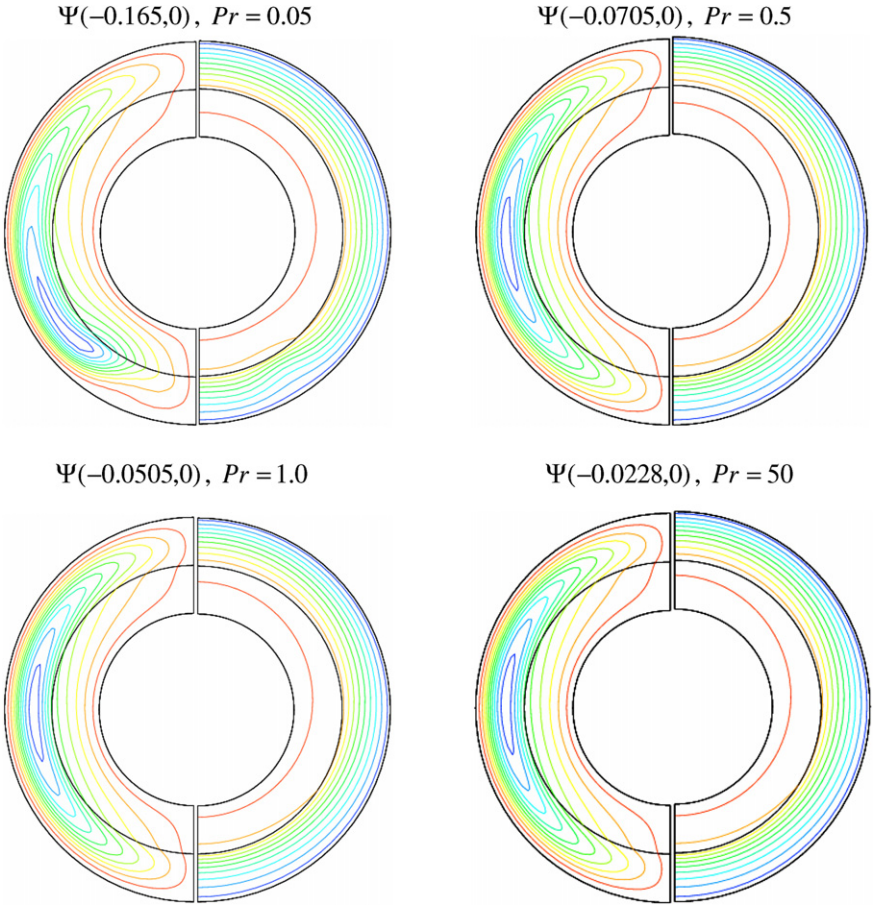

Fig. 14. Effect of varying the Prandtl number on the streamlines and isotherms using $b = 1.5$, $k_s/k_f = 100$, $Da = 10^{-3}$ and $Ra = 10^4$.

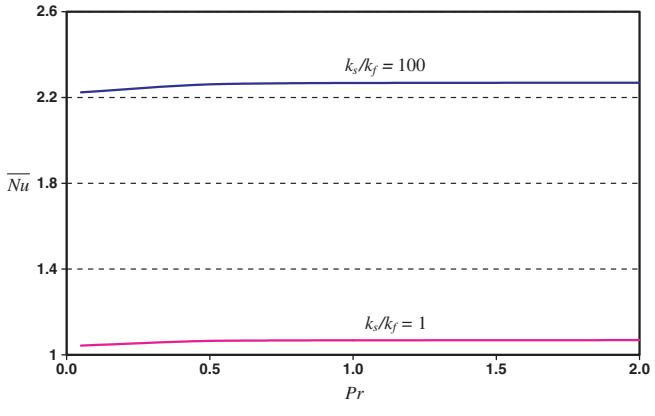

Fig. 15. Effect of Prandtl number on the average Nusselt number for various thermal conductivity ratios using $b = 1.5$, $Da = 10^{-3}$ and $Ra = 10^4$.

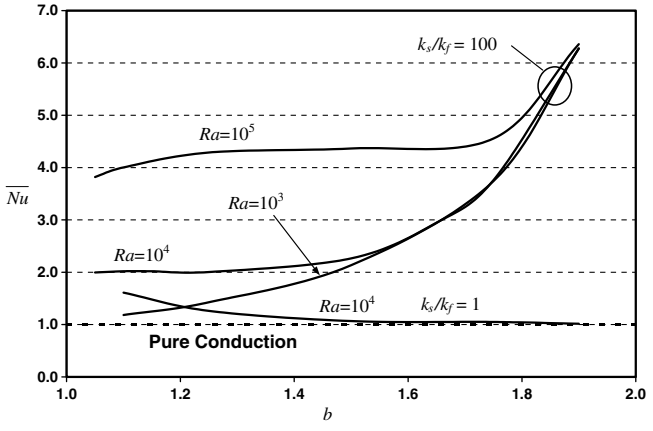

Fig. 16. Effect of porous layer thickness and thermal conductivity ratio for various Rayleigh numbers using $b = 1.5$ and $Da = 10^{-3}$.

i.e., $k_s/k_f = 1$. In fact, the average Nusselt number approaches unity when considering a porous sleeve thickness greater than 1.5, which indicates that the overall heat transfer mechanism has become mainly by conduction heat transfer mechanism. This observation means that thicker porous sleeve lends better insulation effect for $k_s/k_f = 1$.

On the other hand, it is observed from Fig. 16 that the average Nusselt number increases significantly for a porous sleeve with thickness $b > 1.5$ when considering a large thermal conductivity ratio such as $k_s/k_f = 100$. As mentioned earlier, the porous sleeve tends to be more conductive than the fluid layer when incorporating large values of k_s/k_f. As a result, a relatively large temperature gradient is attained across the fluid layer which brings about an appreciated increase in the heat transfer rate. When employing the highest Rayleigh number in this investigation, i.e.,

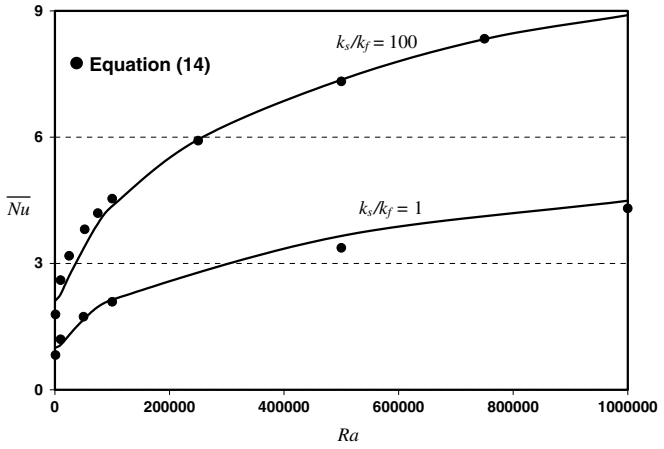

Fig. 17. Comparison of the average Nusselt number between the present numerical results and Eq. (14) for various pertinent parameters.

$Ra = 10^5$, the average Nusselt number is almost uniform for $b < 1.75$. When b exceeds 1.75, however, the average Nusselt number increases remarkably as depicted in Fig. 15. It is worth noting that the average Nusselt number reaches a maximum value for a porous sleeve thickness of $b = 1.9$ for Rayleigh numbers of 10^3, 10^4 and 10^5. This indicates that the maximum predicted Nusselt number depends mostly on the thermal conductivity ratio for a thicker porous sleeve.

Finally, the average Nusselt number calculated along the inner cylinder is correlated over a wide range of various pertinent dimensionless parameters such as Prandtl number $Pr = 0.05$–50, Rayleigh number $Ra = 10^3$–10^6, porous sleeve thickness $b = 1.1$–1.9, Darcy number $Da = 10^{-4}$–10^{-6}, and thermal conductivity ratio $k_s/k_f = 1$–150. This correlation can be mathematically expressed as follows:

$$\overline{Nu} = 0.0166(27.65 + Ra^{0.38})Da^{0.036}Pr^{-0.013}b^{1.07}(k_s/k_f)^{0.17} \quad (14)$$

where the confidence coefficient for the above equation is $R^2 = 94.2\%$. The correlation manifests the significance of Rayleigh number and the dimensionless porous sleeve thickness from the value of their respective exponents. A graphical representation of the above correlation is illustrated in Fig. 17. This figure demonstrates a very good agreement between the numerical results and those obtained by the correlation.

7. Conclusion

Natural convection heat transfer in an annulus partially filled with a fluid-saturated porous medium is studied numerically under steady-state condition. The momentum and energy transport phenomena were explored for various pertinent dimensionless parameters such as the Rayleigh number, porous sleeve thickness, Darcy number, thermal conductivity ratio, and Prandtl number. The inner and outer surfaces of the annulus were maintained at constant temperatures T_i and T_o, respectively, with $T_i > T_o$. In addition, the governing equations were solved using the Galerkin finite element method. The results of this investigation illustrate that Rayleigh number has a significant effect on the overall heat transfer while, on the contrary, Prandtl number has a minimal effect. Moreover, maximum predications of the average Nusselt number are found to depend mostly on the thermal conductivity ratio for a relatively thick porous sleeve as they exhibit better heat transfer rate when considering large thermal conductivity ratios. However, for thermal conductivity ratio of unity, the overall heat transfer rate is found to decreases with an increase in the porous sleeve thickness.

References

[1] M.C. Charrier-Mojtabi, Numerical simulation of two- and three-dimensional free convection flows in a horizontal porous annulus using a pressure and temperature formulation, Int. J. Heat Mass Transfer 40 (1997) 1521–1533.
[2] D.A. Nield, A. Bejan, Convection in Porous Media, third ed., Springer, New York, 2006.
[3] D.B. Ingham, I. Pop (Eds.), Transport Phenomena in Porous Media, vol. III, Elsevier, Oxford, 2005.
[4] K. Vafai (Ed.), Handbook of Porous Media, first ed., Marcel Dekker, New York, 2000.
[5] K. Vafai (Ed.), Handbook of Porous Media, second ed., Taylor & Francis, New York, 2005.
[6] K. Vafai, H. Hadim, Overview of current computational studies of heat transfer in porous media and their applications- natural convection and mixed convection, Adv. Numer. Heat Transfer 2 (2000) 331–371.
[7] D.B. Ingham, A. Bejan, E. Mamut, I. Pop (Eds.), Emerging Technologies and Techniques in Porous Media, Kluwer, Dordrecht, 2004.
[8] A. Bejan, I. Dincer, S. Lorente, A.F. Miguel, A.H. Reis, Porous and Complex Flow Structures in Modern Technologies, Springer, New York, 2004.
[9] J.P. Caltagirone, Instabilities thermoconvectives en milieu poreux, These d'etat, Univ. Pierre et Marie Curie, Paris, VI, France, 1976.
[10] J.P. Caltagirone, Thermoconvective instabilities in a porous medium bounded by two concentric horizontal cylinders, J. Fluid Mech. 65 (1976) 337–362.
[11] J.P. Burns, C.L. Tien, Natural convection in porous media bounded by concentric spheres and horizontal cylinders, Int. J. Heat Mass Transfer 22 (1979) 929–939.
[12] Y.F. Rao, K. Fukuda, S. Hasegawa, Steady and transient analyses of natural convection in a horizontal porous annulus with the Galerkin method, ASME J. Heat Transfer 109 (1987) 919–927.
[13] Y.F. Rao, K. Fukuda, S. Hasegawa, A numerical study of three-dimensional natural convection in a horizontal annulus with a Galerkin method, Int. J. Heat Mass Transfer 31 (1988) 695–707.
[14] W.E. Stewart Jr., A.S. Burns, Convection in a concentric annulus with heat generating porous media and a permeable inner boundary, Int. Comm. Heat Mass Transfer 19 (1992) 859–868.
[15] I. Pop, D.B. Ingham, P. Cheng, Transient natural convection in a horizontal concentric annulus filled with a porous medium, ASME J. Heat Transfer 114 (1992) 990–997.
[16] P. Vasseur, T.H. Nguyen, I. Robillard, V.K.T. Thi, Natural convection between horizontal concentric cylinders filled with a porous layer with internal heat generation, Int. J. Heat Mass Transfer 27 (1984) 337–349.
[17] H.H. Bau, Low Rayleigh number thermal convection in a saturated porous medium bounded by two horizontal eccentric cylinders, J. Heat Transfer 106 (1984) 166–175.

[18] H.H. Bau, Thermal convection in a horizontal, eccentric annulus containing a saturated porous medium – an extended perturbation expansion, Int. J. Heat Mass Transfer 27 (1984) 2277–2287.
[19] J.P.B. Mota, E. Saatdjian, Natural convection in a porous, horizontal cylindrical annulus, J. Heat Transfer 116 (1994) 621–626.
[20] M. Kaviany, Non-Darcian effects on natural convection in porous media confined between horizontal cylinders, Int. J. Heat Mass Transfer 29 (1986) 1513–1519.
[21] J.C. Leong, F.C. Lai, Natural convection in a concentric annulus with a porous sleeve, Int. J. Heat Mass Transfer 49 (2006) 3016–3027.
[22] A. AlAmiri, Analysis of momentum and energy transfer in a lid-driven cavity filled with a porous medium, Int. J. Heat Mass Transfer 43 (2000) 3513–3527.
[23] A. AlAmiri, Natural convection in porous enclosures: the application of the two-energy equation model, Numer. Heat Transfer: Part A 41 (2002) 817–834.
[24] K. Khanafer, K. Vafai, A. Kangarlu, Computational modeling of cerebral diffusion-application to stroke imaging, Magnetic Reson. Imaging 21 (2003) 651–661.
[25] S. Khashan, A. AlAmiri, I. Pop, Numerical simulation of natural convection heat transfer in a porous cavity heated from below using a non-Darcian and thermal non-equilibrium model, Int. J. Heat Mass Transfer 49 (2006) 1039–1049.
[26] C. Taylor, P. Hood, A numerical solution of the Navier–Stokes equations using finite-element technique, Comput. Fluids 1 (1973) 73–89.
[27] P.M. Gresho, R.L. Lee, R.L. Sani, On the time-dependent solution of the incompressible Navier–Stokes equations in two and three dimensions, in: Recent Advance in Numerical Methods in Fluids, Pineridge, Swansea, UK, 1980.
[28] J. Lis, Experimental investigation of natural convection heat transfer in simple and obstructed horizontal annuli, in: Third International Heat Transfer Conference, vol. 2, 1966, pp. 196–204.